Dynamic Stress Stimulates Flow in Fractures: Laboratory Observations of Permeability Enhancement

Jean E. Elkhoury[1†], André Niemeijer[2‡], Emily E. Brodsky[1] and Chris Marone[2]

[1]Dept of Earth and Planetary Sciences, University of California, Santa Cruz.
[2]Dept of Geosciences, Pennsylvania State University, University Park.
[†]Now at Seismological Laboratory, California Institute of Technology, Pasadena.
[‡]Now at Istituto Nazionale di Geofisica e Vulcanologia, Roma, Italy.

Abstract

We report on laboratory experiments designed to investigate the effect of dynamic stressing on permeability of fractured rock. Berea sandstone samples were fractured *in-situ* under triaxial stresses of 10's of MPa, and deionized water was forced through the incipient fracture under conditions of steady and oscillating pore pressure. We find that dynamic stresses produced by pore pressure oscillations induce transient increases in effective permeability. The magnitude of permeability increases scale with the amplitude of pore pressure oscillations, and permeability changes persist well after the stress perturbation. Maximum values of permeability enhancement are 5×10^{-16} m^2 over a background permeability of 1×10^{-15} m^2. Permeability recovery following dynamic stressing occurs as the inverse square root of time. The recovery indicates that a reversible mechanism, such as clogging/unclogging of fractures, as opposed to an irreversible one, like micro fracturing, causes the transient permeability increase. Our data demonstrate the feasibility of dynamically controlling permeability of fractured systems. The result has clear consequences for earthquake dynamic triggering mediated by permeability enhancement in fault zones due to shaking from near and distant earthquakes.

1 Introduction

A wide range of observations show a relation between changes in crustal seismic activity and dynamic stressing produced by shaking from earthquakes [*Coble 1965, Hill et al., 1993, Manga and Wang, 2007*]. The interaction between crustal fluids and the dynamic strains caused by seismic waves is proposed as an explanation for the increase in earthquake activity up to distances of 1250 kilometers from the earthquake generating the seismic waves [*Hill et al., 1993*]. Even common aftershock activity may be related to seismic shaking, as the number of aftershocks per unit fault length is proportional to the amplitude of the seismic waves [*Felzer and Brodsky, 2006*].

Fluid flow seems particular sensitive to seismic waves. The eruption frequency of geysers and flow rates in streams can both increase when shook [*Rojstaczer and Wolf, 1992*; *Muir-Wood and King, 1993; Manga and Brodsky, 2006; Manga et al., 2003; Manga and Wang 2007*]. Seismic waves can also temporarily enhance oil production and spring discharge [*Beresnev and Johnson, 1994; Roberts et al., 2003; Manga et al., 2003*]. Water levels can drop in wells and the tidal phase in fractured reservoirs can decrease [Brodsky et al., 2002; Elkhoury et al., 2006].

Motivated by these observations of transient fluid flow, studies have suggested that seismic waves may increase the permeability in the Earth's crust [*Brodsky et al, 2002; Manga et al., 2003; Roberts et al., 2003; Manga and Brodsky 2006; Elkhoury et al., 2006*]. In order to match the observations, permeability increase must persist after the passage of the seismic waves and be induced by very small strains. Theoretically, a fragile system such as a multiphase fractured rock reservoir could have its permeability increased by the flushing of fluid pathways due to (increased) flow driven in the reservoir by the seismic waves [*Brodsky et al., 2002; Elkhoury et al., 2006*]. However, such a mechanism remains speculative without any direct observation. Furthermore, in the absence of any direct constraints on the micromechanics, predicting the degree of permeability enhancement is challenging.

In this study, we address these gaps in our understanding via laboratory tests. We produced fractures under true-triaxial stresses with fully saturated conditions and then applied sinusoidal oscillations in the upstream pore pressure while holding the downstream pore pressure constant. We measured the permeability of the sample continuously through the experiment and found that the permeability immediately after the oscillations increased systematically with increasing amplitude of the oscillations.

This paper begins with a description of the experimental procedure and raw laboratory results. We then proceed to translate the flow measurements to permeability while addressing some of the complications of fluid flow in porous media such as storage effects. We interpret the resulting permeability enhancements by examining both the repeatability of the permeability recovery and the functional form of the relationship between amplitude and permeability increase. Finally, we briefly discuss the possibilities of extrapolating the results to the field conditions applicable to reservoir engineering and earthquake physics.

2 Experimental Procedure

The goal of our experiments was to measure the permeability response of fractured rock to dynamic stresses created by fluid pressure oscillations. We fractured intact samples within the testing apparatus while flowing fluid through the samples with or without oscillations of the inlet pore pressure (Figure 1). We measured fluid flow rates independently at both the inlet and outlet of the sample, and all stresses, strains, fluid pressures and fluid volumes were measured continuously throughout the experiment. Digital data were collected with a 24-bit system recording at 10kHz.

Each experiment started with an intact, pre-saturated, sample of Berea sandstone (Figure 2a). Samples were L-shaped, jacketed in a latex membrane and placed in the direct shear configuration (Figure 2b). Horizontal and vertical pistons together with a confining pressure loaded the sample. For all

experiments, the normal stress across the fracture plane was 20 MPa and the confining stress was 9 MPa.

The next step in our experiments was to initialize the flow system (Figure 2c). We implemented a pore pressure gradient by applying fluid pressure to the inlet and flushing the system until clear fluid (deionized water) flowed from the outlet. We then connected the second (outlet) pore pressure intensifier, bled trapped air, and applied controlled pressure differential, ΔP, until steady-state flow (i.e. equal flow rates at the inlet and the outlet) was reached. Pore pressures were servo-controlled and applied on line-sources at the inlet and outlet. Line-sources in our experiments consist of 3 point sources aligned in a line covered with 30μm nylon filter paper to avoid clogging of the inlet and outlet at the edges of the incipient fracture.

After fluid flow had reached steady state, we fractured the sample by advancing the vertical piston in displacement control at 5 μm/s, applying load to the top of the sample assembly (Figure 2d). Shear stress was increased on the candidate fracture plane until failure, which was defined as a sudden, large stress drop accompanied by an audible event. Then, we stopped advancement of the vertical piston and maintained constant vertical position.

Once steady state flow was re-established after fracturing, a series of dynamic pore pressure oscillations was initiated (Figure 2e). We imposed sinusoidal pore pressure oscillations and varied amplitude while maintaining constant period and duration (20 sec and 120 sec, respectively). We refer to each set of six oscillations as a dynamic stress test.

Pore pressures at the inlet and outlet were servo-controlled with two independent pressure intensifiers. We measured inlet and outlet flow volumes via linear variable differential transformers (LVDTs) mounted on the intensifier pistons. Mean values of pore pressure were ~3.0 MPa with pressure differential, ΔP, of ~ 0.3 MPa (Table 1). The amplitude, A, of the oscillation ranged from 0.02 to 0.3 MPa. We applied multiple sets of oscillations during a given experiment (Figure 3).

Permeability was inferred via Darcy's Law

$$k = \frac{\mu L}{S}\frac{Q}{\Delta P} \qquad (1)$$

where k is the effective permeability of the fractured sample, μ is viscosity of water, L is flow path and S is the cross-section of the sample. Measured changes in flow rate represent changes in permeability as pore pressure differential, sample volume and water viscosity (i.e. temperature) remain constant and as long as the flow rates at the inlet and outlet are equal. The total effective permeability, k, is used as an interpretive tool to monitor the response of the fracture to the dynamic stresses. Permeability values after the oscillations, k_a, are obtained by averaging the permeability over a 2 sec window starting 10 sec after the oscillation. The 10 sec gap ensures that post-oscillation permeability is not affected by the oscillation itself or by storage effects.

3 Results

We present detailed results from experiments on 4 samples, which were each subjected to multiple sets of pore pressure oscillations (Table 1). In between each set of oscillations, which varied in amplitude, the sample was allowed to recover for up to 100 minutes. We report changes in permeability as $\Delta k = k_a - k_{ref}$, where k_a is effective permeability after the cessation of oscillation and k_{ref} is the initial permeability before dynamic stressing.

We find that pore pressure oscillations (Figure 4a) produce transient increases in the flow rate (Figure 4b) and thus permeability (Figure 5). For each test, we found results like those shown in Figure (5). Permeability exhibits a step increase immediately after the oscillation followed by a gradual recovery (Time t=0 corresponds to initiation of pore pressure oscillations; permeability during pressure oscillations is not shown.)

The striking overlap of permeability derived independently from input and output flows (blue and green curves in Figure 5) demonstrates that the observed change is real and not a transient storage effect associated with the poroelastic response of the system. Storage effects can be observed within the first few seconds after the oscillations and they dissipate within the first 10 seconds after the oscillations. Therefore storage does not affect flow measurements after the oscillations as defined. If water were stored and then squeezed out of the sample, the apparent flow rate would be higher at the outlet. Because the inlet and outlet flow rates, measured independently, are equal, the observed increase and subsequent recovery in flow rate represents a real temporal change in the fracture permeability.

For amplitudes of fluid pressure oscillation in the range 0.02–0.3 MPa, transient increases in permeability, $\Delta k = k_a - k_{ref}$, scales with amplitude (Figure 6). The absolute values of Δk increase are in the range $2\text{x}10^{-18}$ m^2 to $5\text{x}10^{-16}$ m^2, and vary slightly from sample to sample, but the dependence on amplitude is consistent. To compare permeability changes between experiments quantitatively, we normalized changes by k_{ref}. We also normalized the pore pressure amplitude, A, by the pore pressure differential, ΔP, driving the background flow. Figure (6b) shows remarkable similarity between experiments, with all data falling on the same curve given by

$$Log\left(\frac{\Delta \mathrm{k}}{\mathrm{k_{ref}}}\right) = \mathrm{m}\frac{\mathrm{A}}{\Delta \mathrm{P}} - \mathrm{f} \qquad (2)$$

where the slope m = 2.1 with a 95% confidence interval given by [1.7, 2.5], the constant f=1.67 with a 95% confidence interval of [1.5, 1.8] and a goodness of fit measured by an R^2=0.7. Equation (2) is used because it is simple and consistent with the experimental data. However, it is only valid for the range of amplitudes in pore pressure oscillations considered in our experiments. We explore the permeability fit beyond the experimental conditions in section 4.3

To the best of our knowledge, the transient increases in permeability reported here provide the first consistent experimental evidence of flow

enhancement by dynamic stressing. We observe step increases in permeability upon dynamic stressing, followed by gradual recovery (Figure 5) akin to that observed in natural systems (Figure 7) [*Elkhoury et al., 2006*]. Furthermore, the magnitude of the permeability enhancement increases systematically with increasing amplitude of the pore pressure oscillation (Figure 6). A power law fit of the form t^{-p} best represents the recovery of permeability to pre-oscillation values (Figure 5). The exponent p ranges between 0.3 and 1.0 for our suite of experiments. Using p=0.5 as a representative decay results in a slightly reduced, but still acceptable, goodness of fit as discussed in the caption of Figure (9) and subsection 4.1. The square root dependence on time suggests a diffusive process like the migration of pore pressure that would be expected in a porous medium [*Bear, 1979*].

We further probed the system by shearing the fractures to net offsets of 0.6 to 1.3 mm, late in one experiment. The reference permeability was higher for this experiment (p1605) because this sample was not subject to shear immediately after the fracture formed but at a later time during the experiment. The applied shearing decreased the permeability significantly as seen in Figure (8). This provides proof, along with the use of line-sources at the inlet and outlet as shown in Figure (2), that the flow is mostly constrained to the fracture. In the other experiments, the samples were sheared immediately after fracturing, which further reduced permeability and therefore lowered the reference permeability.

The results presented here are a subset of experiments performed on 22 samples to evaluate the permeability response of fractured sandstone subject to dynamic stresses (Table 1). Two additional sets of experiments were conducted. One set involved smooth artificial fractures produced by cutting the rock. The contacting rock faces were ground flat at long wavelength and roughened with polishing compound. Flow rates were fast in this configuration and we were unable to observe reproducible permeability enhancement. The second set of tests considered natural shear fractures, as described in the primary suite of experiments, except that we applied flow-rate boundary conditions at the inlet/outlet and measured the differential pore pressure. One

limitation of this approach was the finite volume of fluid available for flow from the pressure intensifiers (~125 cc, see *Samuelson et al.*, *2008* and *Faoro et al.*, 2009 for additional details). Results of these additional tests were otherwise consistent with the main set of experiments, which we focus on here.

4 Discussion

The increase in permeability induced by oscillatory pore pressure can be explained by a number of mechanisms including microfracturing and clogging/unclogging of fractures. The fact that permeability returns to pre-oscillations values suggests a reversible mechanism, like unclogging and clogging of fractures, is responsible for the observed transient increases in permeability. If an irreversible mechanism like microfracturing is responsible for the permeability enhancement, then an additional mechanism is required to account for permeability recovery. Furthermore, the importance of the initial permeability, k_{ref}, in predicting the permeability changes, reflected in the collapse of all data points in Figure (6b) onto the same curve, indicates a strong memory in the system. It implies that permeability enhancements after a given period of dynamic stressing are not affected by previous excitations. For a complex natural fracture, such as that produced in our experiments, flow is controlled by the geometry of the fracture network, properties of the fracture surface, and wear particles produced during fracture and shear offset. Particle mobilization and subsequent settling and/or agglomeration provides potential coupling between permeability enhancement and dynamic stresses.

The effects of dynamic stressing show that permeability is a dynamically controlled variable. Our result has clear consequences. It demonstrates the feasibility of dynamically controlling permeability of fractured systems. Its application ranges from hydrology and oil reservoir engineering to geophysics and earthquake triggering mediated by permeability enhancement in fault zones due to shaking from near and distant earthquakes.

Our hypothesis of unclogging and clogging is consistent with a step increase in permeability and a gradual recovery as a response to the application

of pore pressure oscillation. Dynamic stresses unclog the fracture and generate a step increase in permeability. As dynamic stressing vanishes, permeability of the system is recovered due to the clogging of the fracture mediated by diffusive processes and settling of fine particles [*Bear, 1979*]. The hypothesis also predicts no permanent changes in permeability, consistent with our data, as well as decreases in permeability given the right conditions. For instance, if sufficient fines are distributed around a critical part of the flow path, then the pore pressure oscillation could cause clogging and decrease the effective permeability. For our full suite of experiments, only one occasion of dynamic stressing in 50 produced a transient decrease in permeability. The sign of shaking-induced permeability changes could vary with rock properties and fracture characteristics, and clearly additional work is necessary to explore this aspect.

4.1 Permeability Recovery

Because we are interested in the permeability response to pore pressure oscillations, we focus on values of permeability before and after oscillations (Figure 5), however, there is additional information in the experiments. Figure (9) shows the permeability recovery after dynamic stressing for two sets of pore pressure oscillations in one experiment. These data allow evaluation of the natural variability in peak permeability enhancement and in recovery among the repeat tests conducted in each experiment. Although there is some variability, the data are generally consistent with power law exponents ranging from 0.3 to 1. A fixed exponent p of 0.5 is an overall reasonable fit to each of the pore pressure oscillations tests (Figure 9). The exponent p could be related to the fractal flow dimension of the fracture, which can vary from oscillation to oscillation [*Walker and Roberts, 2003*]. Therefore, p can be interpreted as the inverse of the dimension, d, of the system, $p \sim 1/d$. Since our samples develop two dimensional shear fractures, the average flow dimension is $d = 2$. Hence $p \sim 0.5$ appears to be a good average exponent value to represent the overall

recovery of the permeability as suggested previously by *Bear*, *1979* and *Barker*, *1988*.

4.2 Flow-driven Permeability Enhancements

Our data indicate an exponential relationship between permeability enhancements (Equation 2) and the amplitude of the applied pore pressure oscillation. The exponential relationship means that permeability increase is proportional to the pre-existing permeability. The easier it is for water to flow through the sample, the greater the permeability increases. This dependency suggests that the mechanism for permeability enhancement may be water flowing through and opening up the fractures. For instance, if the water flow is removing fine particles in the fracture and thus opening up (or widening pathways) new pathways, we might expect that the cross-sectional area of the fracture cleaned would be proportional to the ratio of the excess flow rate over the background flow. In this case, the effective permeability increase would also be proportional to the excess flow and thus

$$\mathrm{d}k_f \propto u_f \qquad (3)$$

where k_f is the permeability in the fracture and u_f is the excess flow in the fracture. According to Darcy's Law, for a fixed path length

$$u_f \propto k_f A \qquad (4)$$

where A is the amplitude of the imposed pressure oscillation. Combining Equations (3) with (2) and integrating results in

$$\ln(k_f) \propto A \qquad (5)$$

as observed. The consistency means that a flow-driven mechanism for permeability enhancements is concordant with a flow-rate threshold for

permeability enhancement. Micromechanically, this flow-rate threshold could be generated through mobilization of fine particles.

4.3 Permeability Fit Beyond the Experimental Conditions

The fit of Equation (2) used in Figure (6b) was restricted to a logarithmic relationship. However, it is only valid for the range of amplitudes in pore pressure oscillations explored. In particular, the relationship is problematic for very small amplitudes. If A=0, Equation (2) has the unphysical behavior that $\Delta k/k_{ref}$ is finite, i.e., there is a permeability increase in the absence of any oscillations. To remedy this problem and extend the correlation beyond the experimental range, we suggest an equivalent relation of the form

$$\frac{\Delta k}{k_{ref}} = a\left(\frac{A}{\Delta P}\right)^{b} \qquad (6)$$

where a=0.7 and b=1.7 are fitting constants and goodness of fit given by an R^2 = 0.88. The opposite limit of a larger value of A relative to ΔP is more problematic. In their present simplified form, neither Equation (2) nor (6) extrapolates successfully to the field data of *Elkhoury et al., 2006*. In the field $A/\Delta P = 10^3$, where A is the amplitude of oscillatory strains provided by seismic waves and the pressure differential ΔP is that of the Earth tides. In contrast, $A/\Delta P = 10^{-1}$ for the experiments presented here. An extrapolation of Equation (6) to the field observations predicts k/k_{ref} ~1000 rather than k/k_{ref} = 3 or 4 as observed [*Elkhoury et al., 2006*]. One alternative is that the ΔP dependence is incompletely captured by the current experiments as the current work explored a range of values of A, not ΔP. Another alternative is introduced by the fact that the field system is clearly more complex than the small-scale laboratory samples. The multiple fractures and highly heterogeneous matrix likely have different composite behavior than a single fracture [*Doan et al., 2007*]. For now,

we note that either Equation (2) or (6) successfully explains laboratory data showing permeability enhancement by dynamic stressing.

5 Conclusions

We observe systematic increases in fracture permeability due to dynamic stressing produced by pore pressure oscillations. We used relatively small peak dynamic stresses (10^{-2} – 10^{-1} MPa) and found permeability changes of up to 50%. Our results show that: 1) permeability enhancements can be reliably and reproducibly induced by dynamic stresses in the laboratory, 2) accurate prediction of the permeability changes requires normalization by the initial permeability of the system, indicating a memory of the initial state of the system, and 3) oscillating the pore pressure results in a logarithmic enhancement, under the experimental conditions considered, which is consistent with a flow-driven mechanism. Mobilization of fine particles and associated clogging/unclogging of the fracture flow path might explain our laboratory observations. Our results point at the possibility of dynamically enhancing the permeability of natural and synthetic systems.

Acknowledgments We gratefully acknowledge experimental support by I. Faoro and J. Samuelson and comments from H. Kanamori and D. Elsworth.

References

Barker, J. A., A generalized radial flow model for hydraulic tests in fractured rock, *Water Resour. Res.*, **24**(10), 1796–1804, 1988.

Bear, J., Hydraulics of groundwater, McGraw-Hill International Book, 1979.

Beresnev, I. A. and Johnson, P. A. Elastic-wave stimulation of oil production: A review of methods and results. *Geophysics* 85, 1000–1017 (1994).

Coble, R.W., The effects of the Alaskan earthquake of March 27, 1964, on ground water in Iowa, *Iowa Acad. Sci*, **72**, 323–332, 1965.

Doan, M., E. E. Brodsky, and D. C. Agnew, Mechanisms of permeability enhancement by seismic waves at Piñon Flat Observatory, in *EOS Trans. AGU Fall Meeting*, vol. **88**, pp. H11B–0481, 2007.

Elkhoury, J. E., E. E. Brodsky, and D. C. Agnew, Seismic waves increase permeability, *Nature*, **441**(7097), 1135–1138, 2006.

Faoro, I., A. Niemeijer, C. Marone, and D. Elsworth, The influence of shear and deviatoric stress on the evolution of permeability in fractured rock, *J. Geophys. Res.*, **114**, B01201, 2009.

Felzer, K. R., and E. E. Brodsky, Decay of aftershock density with distance indicates triggering by dynamic stress, *Nature*, **441**(7094), 735–738, 2006.

Hill, D. P., P. A. Reasenberg, A. Michael, W. J. Arabaz, G. Beroza, D. Brumbaugh, J. N. Brune, R. Castro, S. Davis, D. dePolo, W. L. Ellsworth, J. Gomberg, S. Harmsen, L. House, S. M. Jackson, M. J. S. Johnston, L. Jones, R. Keller, S. Malone, L. Munguia, S. Nava, J. C. Pechmann, A. Sanford, R. W. Simpson, R. B. Smith, M. Stark, M. Stickney, 248 A. Vidal, S. Walter, V. Wong, and J. Zollweg, Seismicity remotely triggered by the magnitude 7.3 Landers, California, earthquake, *Science*, **260**(5114), 1617–1623, 1993.

Manga, M., and E. E. Brodsky, Seismic triggering of eruptions in the far field: volcanoes and geysers, *Annu. Rev. Earth Planet. Sci.*, **34**, 263–291, 2006.

Manga, M., and C. Y. Wang, Earthquake hydrology, in Treatise on Geophysics, vol. **IV**, edited by S. G., pp. 293–320, Elsevier, 2007.

Manga, M., E. E. Brodsky, and M. Boone, Response of stream flow to multiple earthquakes, *Geophys. Res. Lett.*, **30**(5), 1214, 2003.

Muir-Wood, R., and G. C. P. King, Hydrological signatures of earthquake strain, *J. Geophys. Res.*, **98**, 22035–22068, 1993.

Roberts, P., I. B. Esipov, and E. L. Majer, Elastic wave stimulation of oil reservoirs: Promising EOR technology?, *The Leading Edge*, **22**(5), 448–453, 2003.

Rojstaczer, S. and S. Wolf, Permeability changes associated with large

earthquakes: An example from Loma Prieta, California. *Geology*, **20**, 211–214, 1992.

Samuelson, J., C. Marone, B. Voight, and D. Elsworth, Laboratory investigation of frictional behavior of granular volcanic material, *J. Volcano. Geotherm. Res.*, **173**, 265–279, 2008.

Walker, D. D., and R.M. Roberts, Flow dimensions corresponding to hydrogeologic conditions, *Water Resour. Res.*, **39**(12), 1349, 2003.

Parameters	P1605	P1819	P1820	P1830
Failure Shear Stress [MPa]	32	31	31	32
Residual Shear Stress [MPa]	17	16	17	15
Inlet Pore Pressure [MPa]	3.0	3.1	3.2	3.0
Outlet Pore Pressure [MPa]	2.8	2.8	2.8	2.7
Peak Pressure Amplitude [MPa]	0.02 – 0.18	0.03 – 0.25	0.05 – 0.28	0.05 – 0.28
Shear Offset [mm]	0.6	1.0	1.3	0.7
Intact Sample Permeability $x10^{-15}[m^2]$	2.3	2.4	2.3	2.8
k_{ref} $[m^2]$	10^{-15}	10^{-16}	10^{-16}	10^{-16}
Flow Length L [mm]	49.4	49.7	49.8	49.9
Cross-section S $[10^{-3}\ m^2]$	1.28	1.27	1.28	1.28

Table 1: Summary of the four experimental samples, p1605, p1819, p1820 and p1830 showing the similarities in stress conditions and sample dimensions. Viscosity of water, $\mu = 8.89x10^{-4}$ Pa s, is used in Equation (1).

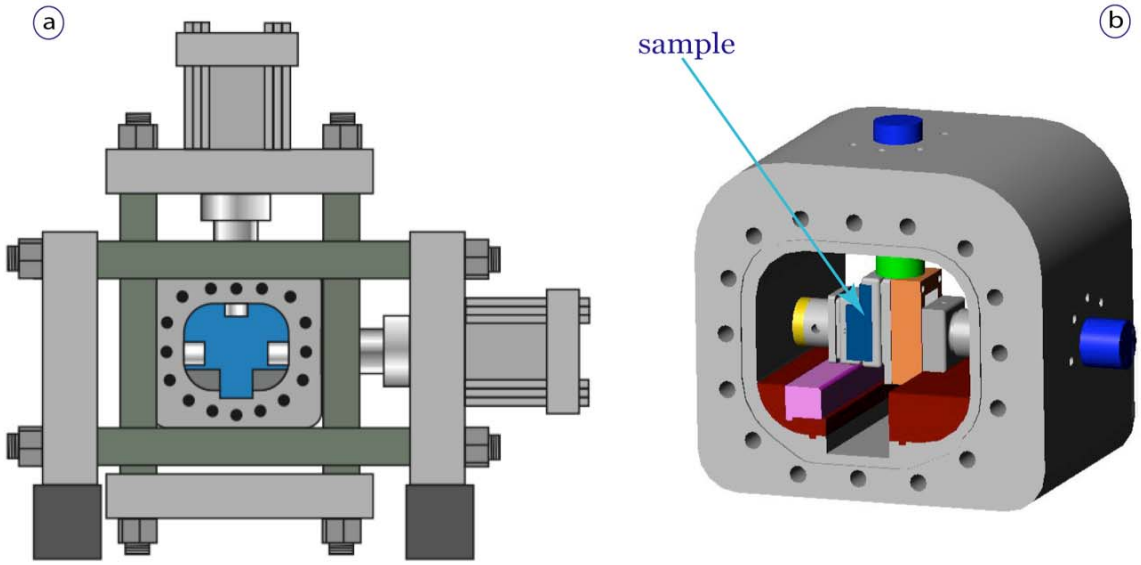

Figure 1: Schematic of the testing apparatus. (a) Loading frame showing horizontal and vertical pistons, which provide normal and shear stresses on the eventual fracture plane, and pressure vessel where confining fluid pressure provides the third stress component. (b) Detail of pressure vessel showing L-shaped rock sample (blue). The single direct shear configuration is used with a frictionless roller-way bearing (orange) to fracture the sample in direct shear under applied load normal to the candidate fracture plane.

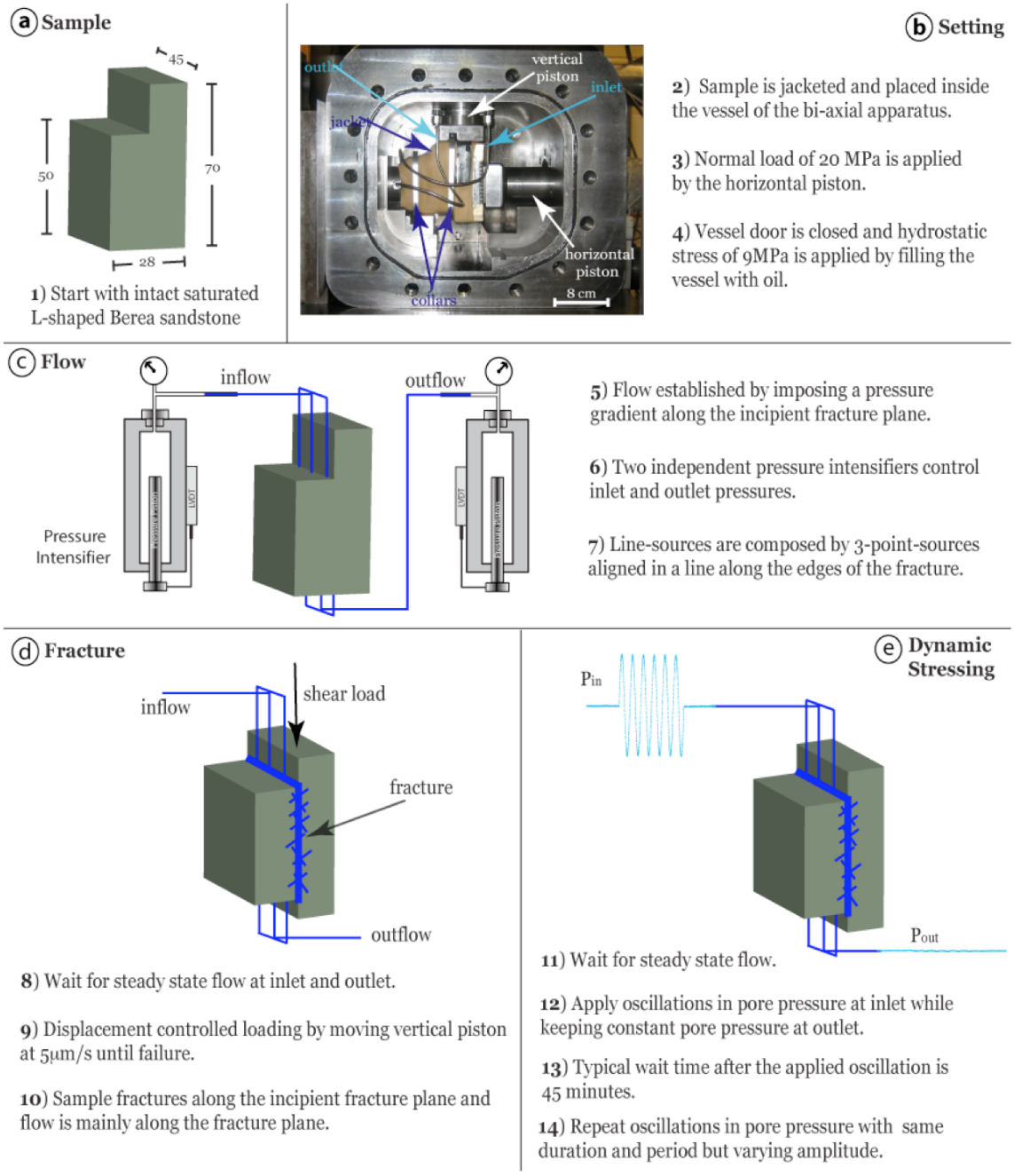

Figure 2: Schematic of the experimental sequence. (a) The sample is intact at the beginning of our experiment. Sample dimensions are in millimeters. The cross area S given in Table 1 is defined by the sample width, 28 mm, and the depth, which is 45 mm. (b) Picture of pressure vessel with door removed to show the sample (within jacket) and loading configuration. The inlet and outlet pipes inside the vessel are connected to the servo-controlled intensifiers (Panel c) through high-pressure fittings in the vessel wall. **(c)** Schematic diagram of

the fluid pressure system for controlled flow through the sample. Independent pressure intensifiers are servo-controlled and can apply constant and variable flow or pressure boundary conditions as a line-source at the top and bottom of the eventual fracture plane. (d) Fractured sample in displacement controlled shear loading in direct single shear configuration. (e) Once steady state is reached, dynamic stressing is applied by means of oscillations in pore pressure at the inlet while keeping outlet pressure constant.

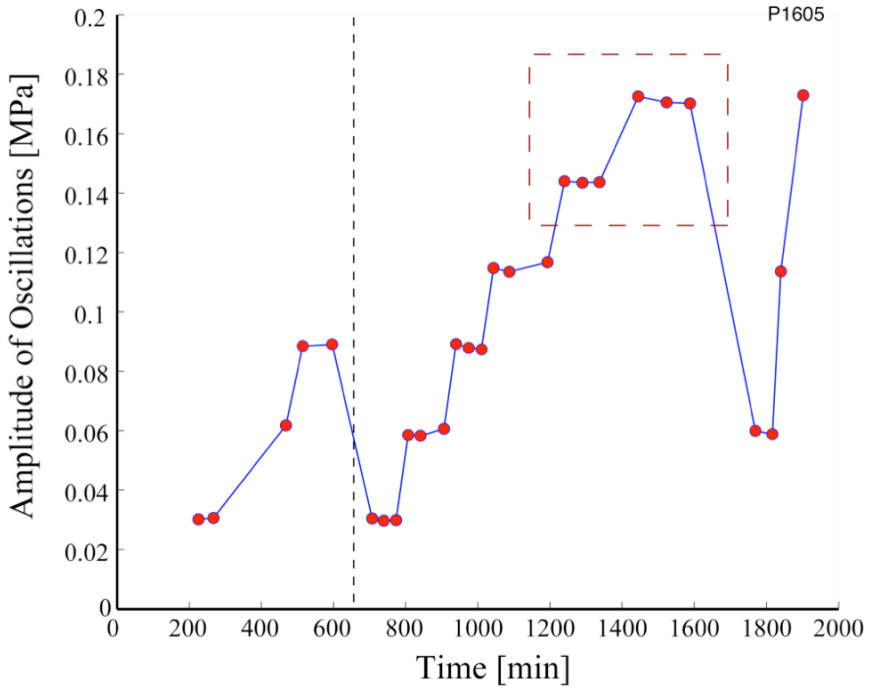

Figure 3: Time sequence of the applied pore pressure oscillations in a complete experiment (p1605). Each point corresponds to one complete set of oscillations: 20 sec period and 120 sec duration. Intervals between tests were typically 30 to 60 minutes. Time=0 corresponds to the point at which the sample fractured. Dashed vertical line shows when fracture was sheared for 600μm at a rate of 5μm/s (Figure 7). Boxed region denotes data shown in Figure (9).

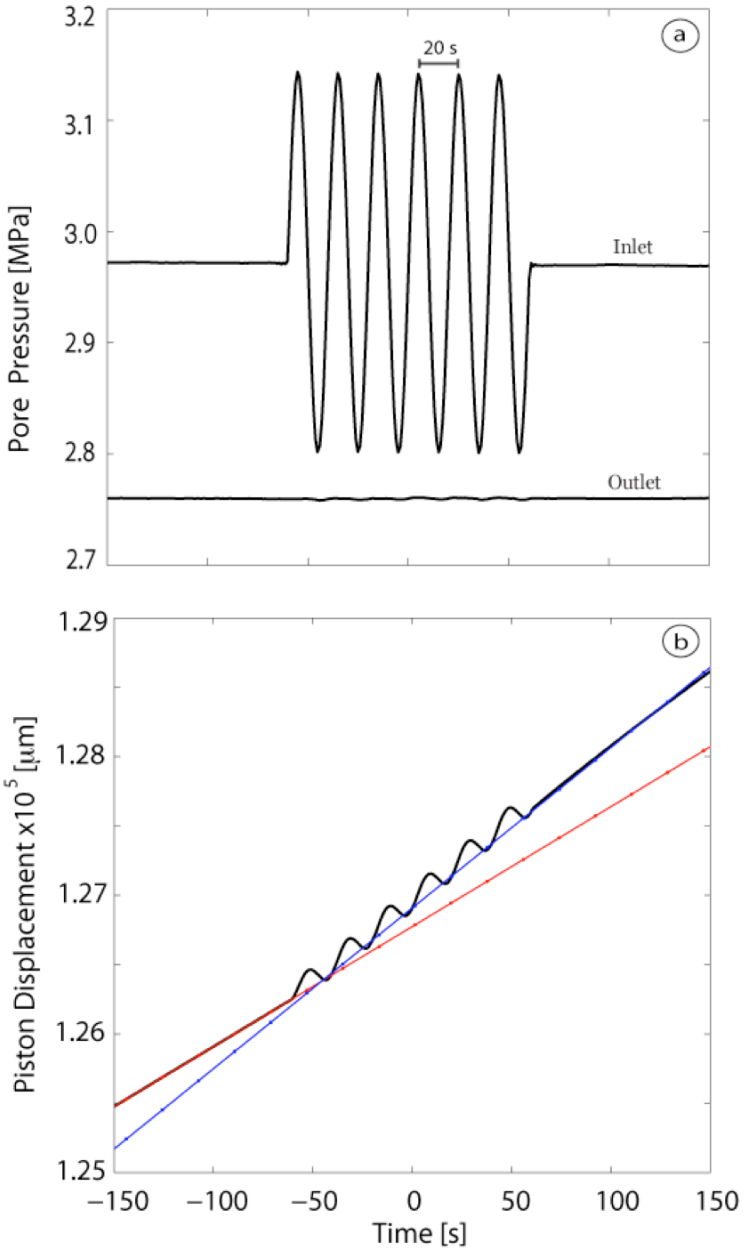

Figure 4: (a) Example of pore pressure oscillations at the flow inlet with fixed pore pressure at the outlet. Pressure conditions before and after the oscillations are identical. (b) Piston displacement recordings at the time of the applied pore pressure oscillation. Piston displacement provides water volume injected through the sample. The slope is effectively flow rate. The increase in flow rate after the oscillation is clear from the increase in the slope after the oscillations (blue) compared to flow rates before oscillation (red).

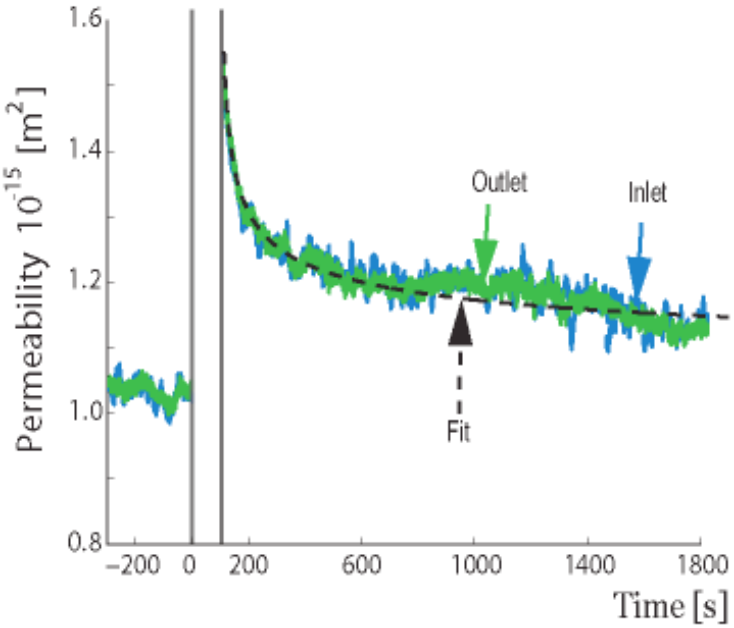

Figure 5: Fluid permeability before and after the pore pressure oscillation. Permeability during the oscillations is not shown (time interval between the two vertical solid lines). The two curves (blue and green) show the permeability measurements based on flow rates obtained independently at the inlet and outlet. The striking overlap obtained from the inlet and outlet demonstrates that the permeability change is real and not related to storage or other poroelastic effects. Permeability shows a step increase followed by a gradual recovery. We use the power law t^{-p}(dashed line) where the exponent p is between 0.3 and 0.7 to fit the permeability recovery (dashed line). We use p = 0.32 in (3b) for a goodness of fit R^2=0.96. If p = 0.5, then R^2=0.7.

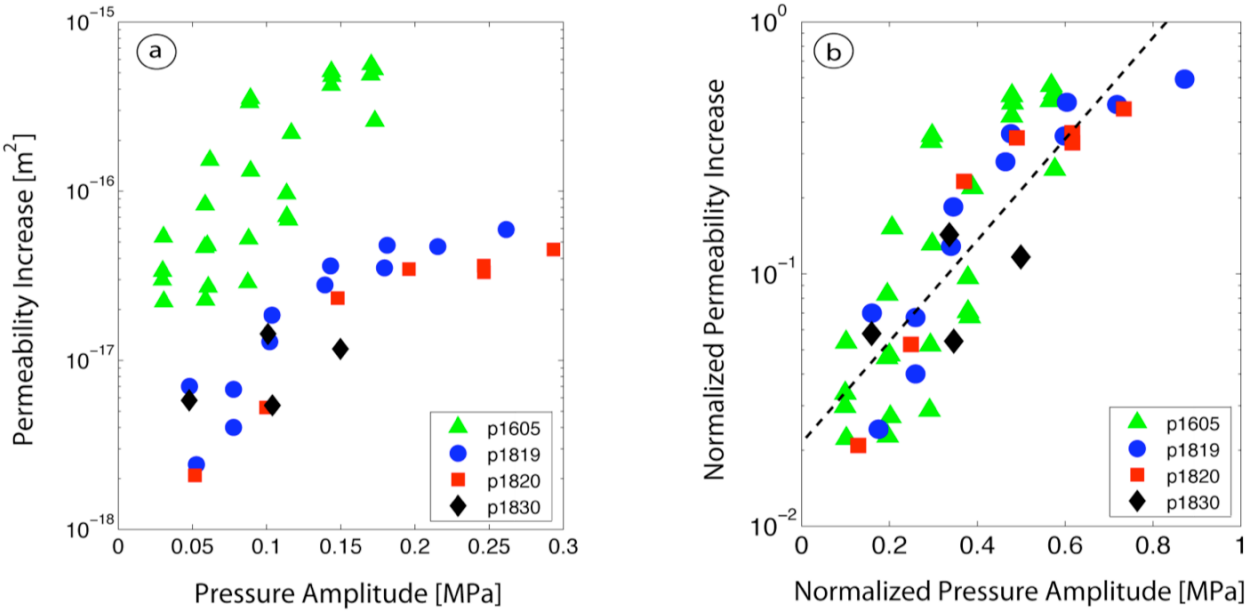

Figure 6: (a) Permeability enhancement, Δk, as a function of pore pressure oscillation amplitude, A. Oscillations were applied in sets of increasing amplitude (Figure 4). Permeability increases by up to 50%. (b) Same data as in (a) except permeability changes are normalized by k_{ref} and the pressure amplitudes are normalized by the pore pressure differential, ΔP, driving the flow. Data collapse onto one curve (dashed line is Equation 2). Note that permeability increases by nearly two orders of magnitude for our range of A values.

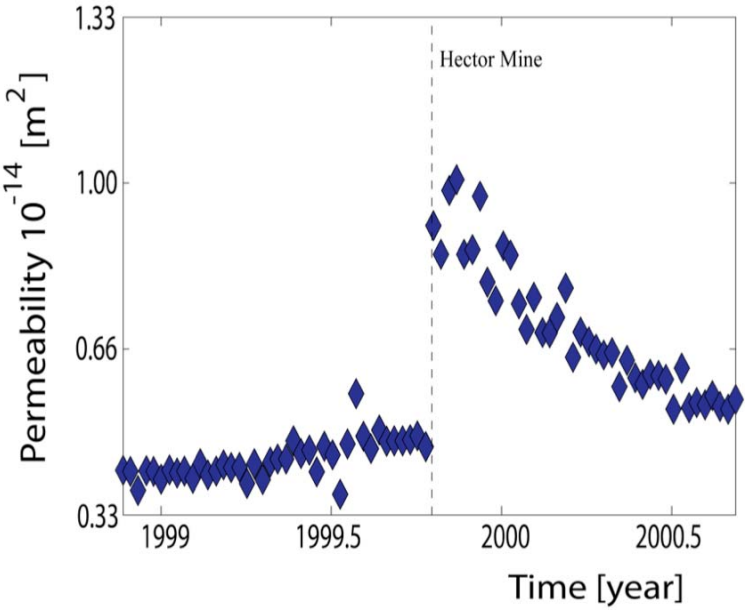

Figure 7: Permeability response to shaking at the Piñon Flat Observatory, in Southern California, from the 1999 Hector Mine earthquake. Notice the clear similarity with Figure 5. Permeability shows a step increase at the time of shaking with a gradual decrease over a time scale of months in contrast to the lab measurements where complete recovery is achieved on the order of hours. (From *Elkhoury et al., 2006*).

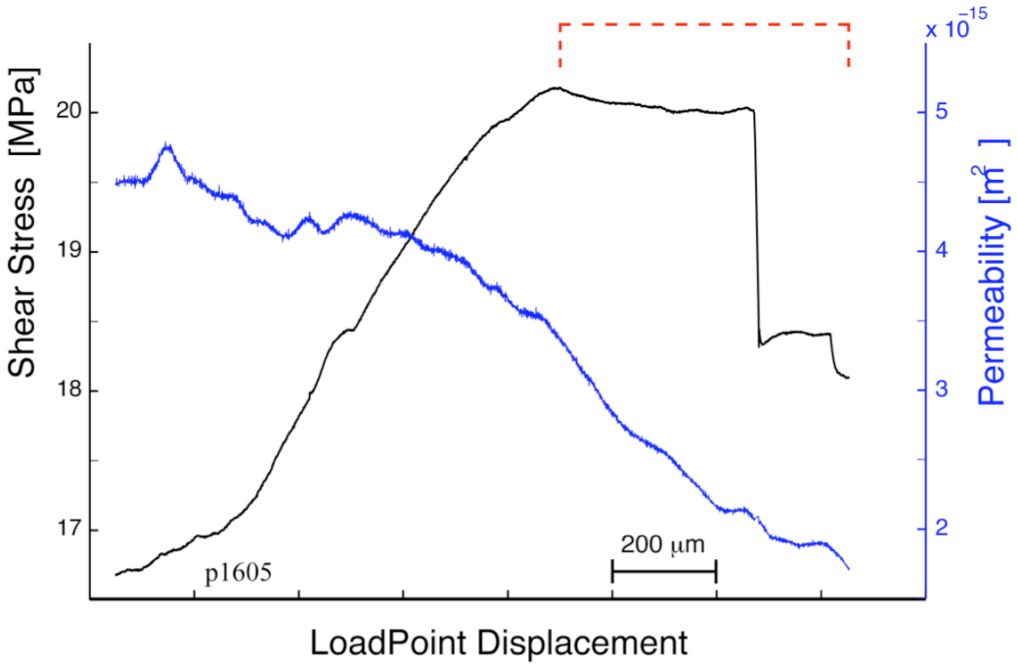

Figure 8: Permeability evolution as a function of shear displacement on the fracture (applied at the time of dashed line in Figure 3). Permeability drops from 4.4 x 10^{-15} m^2 to 1.1x10^{-15} m^2. The near vertical drop in stress represents a stick-slip event. Note small increase in permeability just prior to the stress drop. Dashed bracket indicates the net shear displacement part of the load displacement; ~ 600 μm.

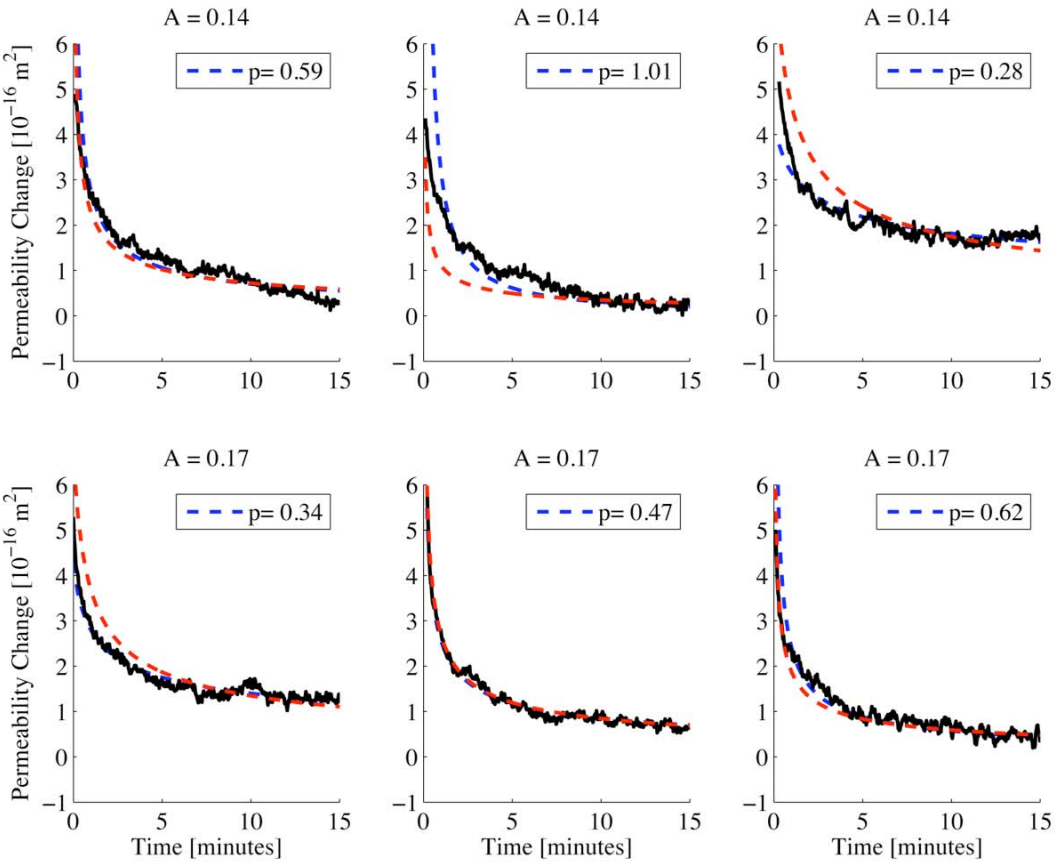

579
580

581 **Figure 9:** Recovery of permeability after the applied oscillation in pore pressure
582 for a subset of oscillations from experiment 1605 (black lines). Y-axes are
583 permeability changes Δk and x-axes are time in minutes after the oscillation.
584 Values of the amplitude of the oscillation, A, are in MPa. Values of p are for the
585 fit of the type t^{-p} (blue dashed lines). Here the exponent ranges from 0.3 to 1.0.
586 Limiting p to 0.5 (red dashed lines) provides a good fit as R^2 ranges between
587 0.7 and 0.9.